Electrowetting-driven droplet shrinkage with tunable focus property*

LIANG Dan, ZHAO Rui, LIANG Zhongcheng**, KONG Meimei, and CHEN Tao**

Center of Optofluidic Technology, College of Optoelectronic Engineering, Nanjing University of Posts and Telecommunication, Nanjing 210023, China

(Received 9 July 2021; Revised 16 August 2021)

In this paper, a non-conductive droplet driven by electrowetting (EW) with planar electrode in surrounding fluid is studied. COMSOL is employed to simulate the evolution of droplet shrinkage and the relative experimental setup is established to monitor the evolution of contact angle and height at different voltages. The droplet contracts inward and the corresponding contact angle/height increase when voltage increases. When the voltage ranges from 50 V to 140 V, the variation of the relative contact angles and height reach up to 118.78° and 3.194 mm, respectively. The system of silicon oil and surrounding liquid propylene glycol (PG) acts as a positive lens, whose focal length varies from 87.153 mm to 42.963 mm.

Document code: A **Article ID:** 1673-1905(2022)03-0166-4

DOI https://doi.org/10.1007/s11801-022-1113-y

In recent years, microfluidics has been widely used in biomedicine[1], electronic printing[2], droplet driving[3] and energy harvesting[4]. Due to the characteristics of easy manufacturing, adaptability to various geometric shapes, short response time, low power consumption, high reversibility, etc, microfluidics-driving droplets have received extensive research and attention. At present, thermal capillary method[5], surface acoustic wave method[6], light induced drive[7], shear air flow drive[8], electrostatic force drive[9], magnetic force method[10] and electrowetting (EW) technology[11-15] are mainly used in microfluidic technology to achieve the purpose of manipulating droplets. Among them, the EW technology has advantages such as faster driving speed, lower power consumption and flexibility, and become the important method for processing surface fluids.

In 1875, LIPPMAN[16] discovered that the position of mercury meniscus in capillary can be controlled when voltages were applied between mercury and an aqueous electrolyte, which is assumed as the basis of EW. In 2004, KUIPER[17] successfully developed a liquid lens composed of two immiscible liquids and applied it in miniature cameras. In 2008, Louisiana State University proposed a planner liquid lens driven by EW[18]. In 2011, MALK et al[19] used a coplanar electrode geometry to observe the rotating flow in an oscillating droplet. The results showed that the increasing oscillation frequency can reduce the oscillation amplitude during the oscillation process. In 2015, WANG[20] reported an annular folded EW liquid lens, its optical power is tripled. In 2019, LEE et al[21] proposed a multifunctional liquid lens driven by EW, which provides both variable focal length and variable aperture function. In 2021, WEN et al[22] introduced the correlation of dynamic contact angle into the numerical model, and studied the droplet detachment process and critical conditions in the EW process.

In this work, a non-conductive droplet on planar electrode is actuated by EW in surrounding fluid. The contact angle and height of the droplet at different voltages are monitored in experiment and are simulated via COMSOL. Series of experiments are carried out to verify the simulation of COMSOL. The results show that the corresponding contact angle and height increase linearly with voltages. When voltages are modulated from 50 V to 140 V, the variation of contact angle achieves 118.78°, and the variation of the droplet height reach up to 3.194 mm. As the system of droplet and surrounding liquid acts as a positive lens, whose focal length varies from 87.153 mm to 42.963 mm. Relevant research will promote the development of EW and further provide reference for the research of liquid lens.

The structure of EW system is shown in Fig.1. The planner electrode is a photoetching indium-tin oxide (ITO) glass (19 mm×24 mm) shown in Fig.1(a). ~5-μm-thick SU8 is spin-coated on the electrode as a dielectric layer, and then ~7 mm diameter fluoropel cytop is coated on the dielectric layer to reduce the friction during movement of the droplet. About 30 μL phenylmethyl silicone oil droplet is dropped onto the specific area, which is surrounded by immiscible conductive

* This work has been supported by the National Natural Science Foundation of China (No.61775102), and the Youth Program of National Natural Science Foundation of China (No.61905117).

** E-mails: zhaor@njupt.edu.cn; zcliang@njupt.edu.cn

liquid (propylene glycol (PG) containing with 1wt% tetrabutylammonium chloride (TBAC)). The relevant parameters are listed in Tab.1 (at room temperature 20 ℃).

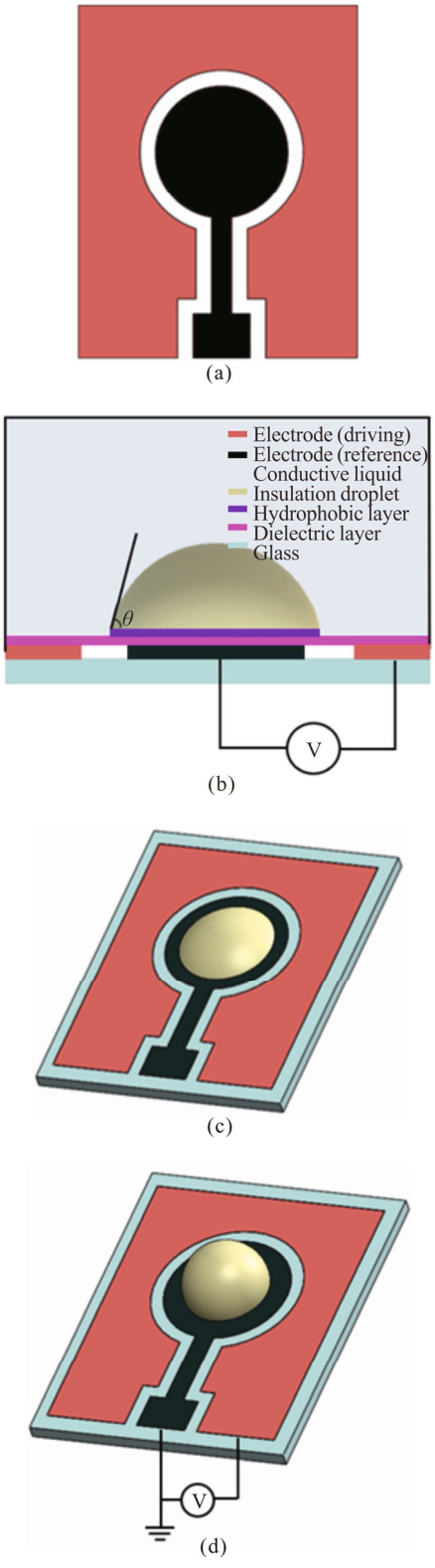

Fig.1 Structure drawing of EW system: (a) Structure of planar electrode; (b) The cross-section view of EW; (c) Initial state *U*=0 V; (d) Working state *U*≠0 V

Tab.1 Parameters of liquid media

	Phenylmethyl silicon oil	PG
Density (g/cm^3)	~1.08	~1.035
Dielectric constant	~2.6—3.0	~22
Refractive index	~1.48	~1.43
Surface tension (mN/m)	~21—28.5	~38
Viscosity (mPa·s)	~50—80	~56

A sinusoidal alternating current (AC) signal generated by a function generator is amplified by a power amplifier, whose frequency is 500 Hz. When the voltage is zero (U=0 V), the droplet shape is assumed to be spherical since the two liquids have the same density approximately, which is shown in Fig.1(c). When voltage is applied, the droplet begins to contract inward shown in Fig.1(d). Fig.2 provides the schematic diagram of the contact angle measurement of droplet.

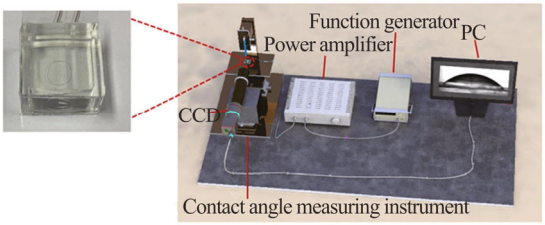

Fig.2 Schematic diagram of the measurement system

Column (a) in Fig.3 provides the profile evolution of silicon oil droplet captured by SCI3000F (shown in Fig.2) at 0 V, 60 V, 80 V, 100 V, 120 V and 140 V, respectively, while column (b) in Fig.3 shows the corresponding profiles of droplet at different voltages simulated by COMSOL. Here COMSOL Multiphysics 5.4(a) is employed to simulate the evolution of EW-driven droplet shrinkage, and the related parameters are provided in Tab.2. It is easy to find that the simulated profile of droplets at different voltage coincides with that in experiment, the wettability of the conductive liquid on the solid surface is changed in term of EW theory, consequently the shape of the insulating droplet changes with it[23].

Fig.4 illustrates the contact angle and the height of droplet versus working voltage measured in experiment, which are repeated 3 times at fresh sample. When the voltage is in the range of 0—50 V, no obvious change appears in droplet profile. We define that the droplet is in the static state, and 50 V is the threshold voltage. The authors assume that the existence of threshold voltage is mainly caused by the pinning effect of EW[24]. Above the threshold voltage, the droplet starts to contract inward and visible change of contact angle and height for the silicon droplet can be observed. Continuously increase voltage, the contact angle and the height increase with voltage linearly. When the voltage is 140 V, the equilibrium

contact angle is 118.78° and the relevant stable height is 3.194 mm. As shown in Fig.4, the variation of contact angle and the relative height increased by approximately 72° and 1.68 mm, respectively when the voltage is increased from 50 V to 140 V.

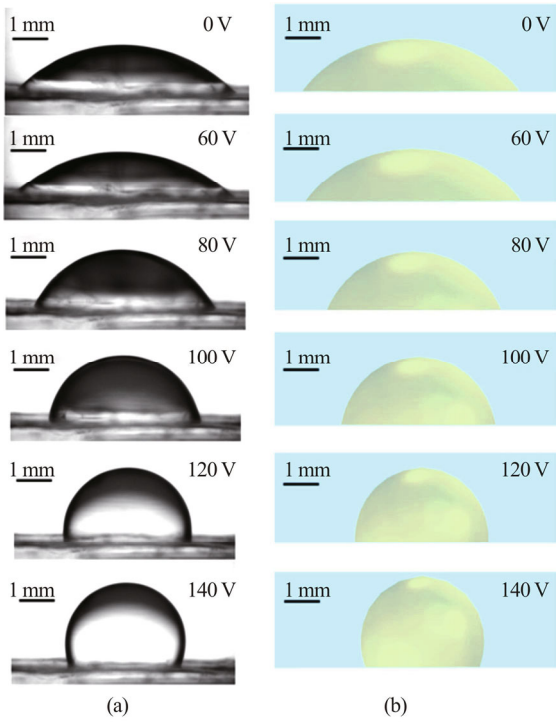

Fig.3 Comparison of droplet profiles at different voltages in (a) experiment and (b) simulation

Tab.2 Parameters of simulation model

Parameter	Value	Instruction
θ (°)	45	Zero voltage contact angle
γ (mN/m)	12.5	Surface tension
ε_r	19	Dielectric constant difference

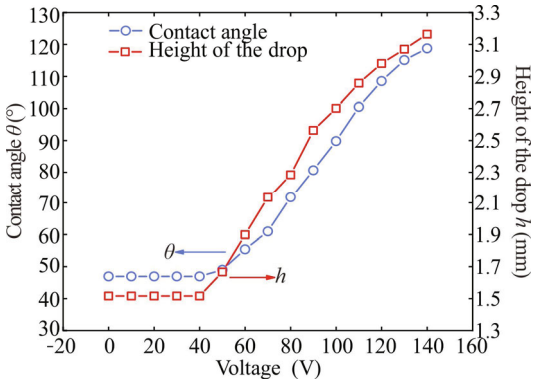

Fig.4 The contact angle and height of droplet versus voltage

Since the refractive index of silicone oil droplet is larger than that of the conductive liquid, and its profile is changed with the working voltage, the system of silicon oil droplet and surrounding liquid PG acts as a various focus positive lens.

Fig.5 shows the sequential images "A" imaged by the system mentioned above at different voltages. As the voltage increases, the boundary of the silicone oil droplet shrinks, the contact angle and the height of the droplets are both increased. When working voltage is 60 V, an initially blurred image "A" is partially clear shown in Fig.5(a) and (b). The images "A" are both magnified and gradually clear when 80 V and 100 V are applied to the EW system in Fig.5(c) and (d). Its zoom performance is measured by the autofocus detection instrument[25].

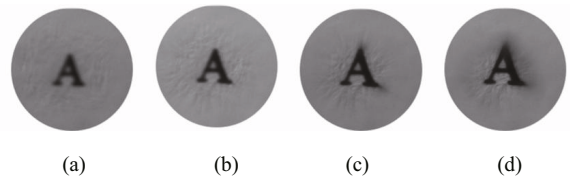

Fig.5 Captured images at different voltages: (a) *U*=0 V; (b) *U*=60 V; (c) *U*=80 V; (d) *U*=100 V

Fig.6 is the variation of the relative focal length of the EW system at different voltages, where the line with hollow square is theoretical value while the line with hollow circle is measured in experiment. As expected, the focal length of our system decreases from 87.153 mm to 42.963 mm when voltage increases from 50 V to 140 V.

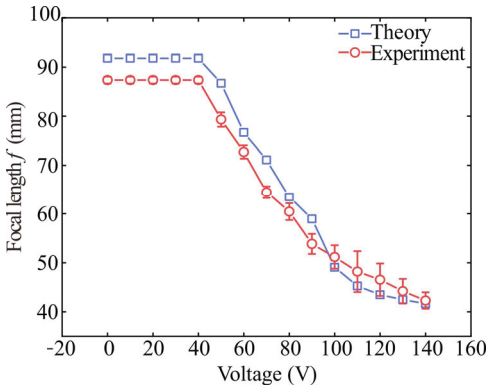

Fig.6 Relationship between focal length and voltage

The focus of this work is to study the shrinkage of non-conductive droplet on planar electrode in surrounding fluid actuated by the EW. The profile evolution of droplets at different voltages is monitored in experiment and simulated by COMSOL. When the voltage is less than 50 V, the droplet is in a static state. When the voltage is in the range from 50 V to 140 V, the relative variation of contact angle and height reach 118.78° and 3.194 mm, respectively. The various focal length of the EW system ranges from 87.153 mm to 42.963 mm.

Statements and Declarations

The authors declare that there are no conflicts of interest related to this article.

References

[1] ZHONG Q F, DING H B, GAO B B, et al. Advances of microfluidics in biomedical engineering[J]. Advanced materials technologies, 2019, 4(6)：1800663.

[2] WEISGRAB G, OVSIANIKOV A, COSTA P F. Functional 3D printing for microfluidic chips[J]. Advanced material technologies, 2019, 4(10)：1900275.

[3] CHOU W L, PEE Y L, YANG C L, et al. Recent advances in applications of droplet microfluidics[J]. Micromachines, 2015, 6(9)：1249-1271.

[4] CONNER C, VISSER T, LOESSBERG J, et al. Energy harvesting with a liquid-metal microfluidic influence machine[J]. Physical review applied, 2018, 9(4)：044008.

[5] DARHUBER A, VALENTINO J, TROIAN S. Planar digital nanoliter dispensing system based on thermocapillary actuation[J]. Lab on a chip, 2010, 10(8)：1061-1071.

[6] HERON S, WILSON R, SHAFFER S, et al. Surface acoustic wave nebulization of peptides as a microfluidic interface for mass spectrometry[J]. Analytical chemistry, 2010, 82(10)：3985-3989.

[7] CHEN R, JIAO L, ZHU X, et al. Cassie-to-Wenzel transition of droplet on the superhydrophobic surface caused by light induced evaporation[J]. Applied thermal engineering, 2018, 144：945-959.

[8] HU H, HUANG S, CHEN L. Displacement of liquid droplets on micro-grooved surfaces with air flow[J]. Experimental thermal & fluid science, 2013, 49：86-93.

[9] WASHIZU M. Electrostatic actuation of liquid droplets for micro-reactor applications[J]. IEEE transactions on industry applications, 1998, 34(4)：732-737.

[10] TIMONEN J, LATIKKA M, LEIBLER L, et al. Switchable static and dynamic self-assembly of magnetic droplets on superhydrophobic surfaces[J]. Science, 2013, 341(6143)：253-257.

[11] ZHAO R, LIANG Z C. Mechanism of contact angle saturation and an energy-based model for electrowetting[J]. Chinese physics B, 2016, 25(6)：364-369.

[12] MUGELE F, BARET J C. Topical review：electrowetting：from basics to applications[J]. Journal of physics condensed matter, 2005, 17(28)：705-774.

[13] VANCAUWENBERGHE V, MARCO P D, BRUTIN D. Wetting and evaporation of a sessile drop under an external electrical field：a review[J]. Colloids & surfaces a physicochemical & engineering aspects, 2013, 432(17)：50-56.

[14] GRINSVEN K V, ASHTIANI A O, JIANG H. Fabrication and actuation of an electrowetting droplet array on a flexible substrate[J]. Micromachines, 2017, 8(11)：334.

[15] NELSON W C, KIM C J C, CHANG J. Droplet actuation by electrowetting-on-dielectric (EWOD)：a review[J]. Journal adhesion science & technology, 2012, 26(12-17)：1747-1771.

[16] LIPPMANN G. Relations entre les phenomenes electriques et capillaires[J]. Annales chimie physique, 1875, 5(11)：494.

[17] KUIPER S. Variable-focus liquid lens for miniature cameras[J]. Applied physics letters, 2004, 85(7)：1128-1130.

[18] LIU C X, PARK J, CHOI J W. A planar lens based on the electrowetting of two immiscible liquids[J]. Journal of micromechanics & microengineering, 2008, 18(3)：035023.

[19] MALK R, FOUILLET Y, DAVOUST L. Rotating flow within a droplet actuated with AC EWOD[J]. Sensors & actuators B chemical, 2011, 154(2)：191-198.

[20] LEI L, CHAO L, REN H, et al. Annular folded electrowetting liquid lens[J]. Optics letters, 2015, 40(9)：1968-1971.

[21] LEE J, PARK Y, CHUNG S K. Multifunctional liquid lens for variable focus and aperture[J]. Sensors & actuators A physical, 2019, 287：77-184.

[22] WENG N, WANG Q, GU J, et al. The dynamics of droplet detachment in reversed electrowetting (REW)[J]. Colloids and surfaces a physicochemical and engineering aspects, 2021, 616(4)：126303.

[23] ZHANG W J, ZHAO R, HE Y J, et al. Electrowetting-actuated optofluidic phase modulator[J]. Optics express, 2021, 29(2)：797-804.

[24] LIN Y Y, EVANS R D, WELCH E, et al. Low voltage electrowetting-on-dielectric platform using multilayer insulators[J]. Sensors & actuators B chemical, 2010, 150(1)：465-470.

[25] CHEN T. Research on microfluidic optical information device and its application[D]. Nanjing：Nanjing University of Posts and Telecommunications, 2015：54-56. (in Chinese)